Catalysis Today 432 (2024) 114570

Contents lists available at ScienceDirect

Catalysis Today

journal homepage: www.elsevier.com/locate/cattod

Catalytic oxidation of volatile organic compounds with Mn-zeolites

L. Toloza-Blanco [a], K. Góra-Marek [b], K.A. Tarach [b], J. Sobalska [b], J. Martínez-Triguero [a], A. Plá-Hernández [a], A.E. Palomares [a,*]

[a] Instituto de Tecnología Química, Universitat Politècnica de València - Consejo Superior de Investigaciones Científicas (UPV-CSIC), Valencia, Spain
[b] Faculty of Chemistry, Jagiellonian University in Kraków, Gronostajowa 2, Kraków 30-387, Poland

ARTICLE INFO

Keywords:
VOCs
Mn-zeolites
Air pollution
Catalytic oxidation
Ethanol

ABSTRACT

Mn-catalysts supported on zeolites are active materials for oxidising volatile organic compounds, but the catalysts' activity and selectivity depend on the support's characteristics. In this work, we study the performance of different Mn catalysts supported on zeolites with different Si/Al ratios and topology in the ethanol oxidation reaction. The results show a correlation between the mechanism of the reaction and the presence or absence of acid sites on the zeolite surface, which is based on its aluminium content. It is observed that the presence of Brønsted acid sites catalyses ethanol dehydration to ethylene that is oxidised to CO_2 at higher temperatures. Without protonic acid sites, ethanol is primarily oxidised to acetaldehyde and subsequently oxidised to CO_2, achieving a complete oxidation at lower temperatures. The acidity also influences the nature of the metallic active sites, forming Mn-oxo species with higher oxidation state in the catalyst with lower aluminium content. These species are more active than those formed in the catalyst enriched with Brønsted acid sites. Thus, zeolites with higher Si/Al ratios are more adequate for supporting Mn catalysts in the ethanol oxidation reaction. The results show that low acidity is a decisive factor in designing active catalysts for this reaction, while zeolite topology or catalyst surface area are of secondary importance.

1. Introduction

Volatile organic compounds (VOCs) are main air pollutants and their properties and uses depend mainly on the functional groups that appear in the molecule. Oxygen-containing VOCs, like alcohols, are commonly used in cosmetics and personal care products, e.g. perfumes, hair spray, aerosols, etc. and domestic and industrial products, e.g. varnishes, window cleaners, paint thinners, and adhesives [1]. The wide use of these substances results in the emission of many VOC pollutants. They can produce photochemical oxidants [2], have negative impact in people's health and at high concentration may even cause central nervous system depression [3]. In particular, ethanol maximises the formation of aldehydes, which cause irritation, breath shortness, mucous membrane irritation, and chest tightness [3,4]. It is a major indoor pollutant emitted from different materials and trapped in airtight buildings [5,6]. It is also widely used in the chemical industry and as a fuel additive in a high-demand global market. [7,8]. Therefore, the development of efficient systems for removing ethanol and its derivatives from automobile exhausts, chemical industry and indoors is an essential challenge for society.

The best available technologies for VOCs control are adsorption or thermal/catalytic oxidation. Thermal incineration is the conventional method of controlling VOC emissions from industrial processes and is successfully used in many processes, but it is not free of some drawbacks. For example, the poor efficiency at low concentrations and the high temperature necessary for the complete oxidation results in significant energetic expenses and the generation of other pollutants such as NO_x. Catalysis has a role in this field [9] as the oxidation of the pollutants is achieved at lower temperatures, decreasing the energetic cost and the formation of NO_x.

The use of catalysts based on noble metals [10,11] has been proposed for VOCs oxidation, but their sensitivity to poisons, the price and scarceness encourage their replacement. Perovskites and transition metal oxides, such as ceria, manganese, nickel, cobalt and copper oxides, have also shown catalytic activity for VOCs oxidation [10–15]. Catalytic beds based on metals or metal oxides supported on porous solids are active in low-temperature ranges, managing to oxidise VOCs with high efficiencies to CO_2 and H_2O [16,17]. Manganese is an interesting material among the different transition metals due to its low price, availability and its variable valence states that makes it adequate for

* Corresponding author.
E-mail address: apalomar@iqn.upv.es (A.E. Palomares).

https://doi.org/10.1016/j.cattod.2024.114570
Received 15 December 2023; Received in revised form 29 January 2024; Accepted 5 February 2024
Available online 7 February 2024

oxidation reactions [18]. Manganese oxides have been used to oxidise ethanol, revealing different adsorption-oxidation sites by various reaction mechanisms [19,20]. Manganese oxides with different morphology and crystal faces were studied by Men et al. [21], showing that morphology may enhance catalytic performance probably due to the formation of more surface Mn^{4+} and active oxygen species. The latter can also be achieved by preparing MnO_2 with a three-dimensional ordered mesoporous structure [22] or preparing the catalysts by an exotemplating approach [23]. Adding a basic promoter, such as K, Ca, or Mg, to Mn_3O_4 promotes the catalytic activity, probably due to the formation of defect-oxides or hydroxyl-like groups [24]. Mn-based oxides can be classified into four types: single, supported, composite, and special crystalline manganese oxides [25]. Supported materials are common catalysts used in different catalytic reactions for environmental applications [26–29] as the supports increase the surface area of the catalysts, improve the metal dispersion, favour the adsorption of the reactants and may be active in the oxidation reaction. The main supports used for manganese are active carbon, alumina, titania, and ceria [24,25,30]. However, to the best of our knowledge, the use of Mn supported on zeolites as catalysts for this reaction has not been reported even though zeolites are common catalysts or catalyst supports due to their high surface area, ion exchange capacity and acid properties [17,31]. Hereby, we study the performance of manganese supported on zeolites for the oxidation of VOCs using ethanol as a model molecule. The reaction was scrutinised by linking catalytic results with comprehensive spectroscopic data obtained by *in situ* and *operando* FT-IR and UV–vis techniques.

2. Experimental

2.1. Catalyst preparation

Catalysts were prepared using commercially available MFI (Zeolyst, CBV2314 Si/Al=11.5, Zeocat PZ-2/1000 Si/Al=1000) and BEA (Zeolyst CP814C Si/Al=19) zeolites. Different aqueous solutions of a manganese precursor, $Mn(CH_3COO)_2{\cdot}4\ H_2O$, were added by the wet impregnation method to obtain the desired manganese content in the final catalyst (5 wt%). After impregnation, the catalyst was dried at 100 °C for 24 h and calcined in air at 550 °C for four hours with a heating rate of 10 °C·min^{-1}. Finally, the catalysts were pelletised, crushed, and sieved to obtain grains with a 0.25−0.45 mm diameter.

2.2. Catalytic tests

Catalytic tests were conducted in a conventional fixed-bed quartz reactor at atmospheric pressure. The catalyst bed (2 g) was supported on a quartz plug in the reactor. Silicon monocarbide (>0.42 mm o.d.) was placed above the catalyst bed as a preheating zone of the incoming feed stream. The temperature was measured with a K-thermocouple inside the reactor. The reactor was housed in an electrically heated furnace. Before the reaction, the calcined catalyst was activated at 250 °C with air for 30 min.

The gas mixture, composed of ethanol (1000 ppm) and dry air, was introduced into the reactor at 400 mL·min^{-1} (GHSV = 15,000 h^{-1}) and with a residence time of 0.24 s. The reaction was carried out under a continuous flow of reactants, and each catalyst was tested at increasing temperatures, i.e. 150, 200, 230, 260, 300, 350, and 400 °C, for 20 min. The reaction products were identified and quantified using a gas chromatograph Varian 3600 with flame ionisation (FID) and a thermal conductivity detector (TCD). The concentration of ethanol and any other product formed in the reaction was determined on the FID after separation in an Rt-Q-Bond PLOT 30 m, 0.32 mm, 10 microns ID GC column. CO and CO_2 were determined in the TCD detector after separation in a ShinCarbon ST Micropacked, 80/100, 1 m, 0.53 mm ID and a MolSieve 13X, 80/100, 1.2 m, 1/16", 1 mm ID CP1309 GC columns.

2.3. Characterization studies

The chemical composition was measured by inductively coupled plasma (ICP-OES) in a Thermo Scientific™ iCAP PRO ICP-Optical Emission Spectrometer. Before analysis, 40 mg of each calcined sample was dissolved with concentrated hydrofluoric and nitric acid solution.

Textural properties of the catalysts were determined at −196 ºC by N_2 adsorption with a Micromeritics ASAP 2040 device. The samples (0.2 g) with a particle size between 0.4 and 0.6 mm were pretreated at 200 °C for five hours at high vacuum. Surface areas were obtained by the BET method.

X-ray diffraction (XRD) patterns were recorded in a PANalytical CUBIX diffractometer equipped with a PANalytical X'Celerator detector. X-ray radiation of Cu Kα ($\lambda1 = 1.5406$ Å, $\lambda2 = 1.5444$ Å, I2/I1 = 0.5) was used with a tube voltage of 45 kV and with an intensity of 40 mA.

Temperature-programmed reduction (TPR) studies were performed using a Micromeritics Autochem 2910 automated chemisorption analysis instrument. The reduction of the samples (10–20 mg) was conducted from 40 to 600 °C with a thermal ramp of 10 °C·min^{-1} using an Ar: H_2 flow (10% H_2) of 50 mL·min^{-1}.

High-resolution field emission scanning electron microscopy (HRFESEM) measurements were made in a ZEISS GeminiSEM 500, which was equipped with a secondary electron (SE2) and an energy-dispersive X-ray spectroscopy (EDS) detector. The micrographs were acquired with a constant accelerating voltage (1.5 kV) and different magnifications.

X-ray photoelectron spectroscopy (XPS) analysis was performed with a SPECS spectrometer equipped with a Phoibos 150 MCD-9 multichannel analyser using a monochromatic Al Kα (1486.6 eV) X-ray source. Spectra were recorded using an analyser pass energy of 30 eV (X-ray power of 100 W). During data processing of the XPS spectra, binding energy (BE) values were referenced to C *1 s* peak (284.5 eV). CasaXPS software has been used for spectra treatment.

The acidity of the samples was measured by adsorption-desorption of pyridine on self-supported sample wafers, followed by infrared spectroscopy in a Nicolet 710 FT IR spectrometer. The wafers were activated at 350 °C under vacuum for two hours. After activation, pyridine vapour was adsorbed into the samples. Desorption of pyridine under vacuum was measured at 150, 250 and 350 °C, followed by an IR measurement at room temperature. The data were treated using Omnic™ Series software and normalised according to the sample weight. The Brønsted (BAS) and Lewis (LAS) acid sites concentration were obtained from the integrated area of the adsorbed pyridine bands at 1560–1535 (pyridinium ions, PyH^+) and 1440 – 1460 cm^{-1} (Py-Lewis site adduct) by using extinction coefficients reported earlier [32]. The acid strength was assessed by pyridine thermodesorption and presented as the A_{250}/A_{150} and A_{350}/A_{150} ratios. These ratios are intensities of PyH^+ ions band upon the desorption at 250 °C (or 350 °C) and evacuation at 150 °C, respectively, and express the ratio of pyridine molecules neutralising protonic sites that survived desorption at 250 °C (or 350 °C).

FT-IR *in situ* experiments were carried out with a Bruker InvenioX spectrometer, using self-supported pellets (5 mg·cm^{-2}) placed in a quartz custom-made IR cell. Before the experiments, the materials were evacuated at 350 °C (with a rate of 5 °C/min) for one hour under a vacuum (10^{-5} mbar) to remove all adsorbed species. Upon admission of 20 Torr of oxygen, the samples were heated at 550 °C for 30 min, then evacuated under high vacuum conditions and cooled down to room temperature or 250 °C for *in situ* standard or rapid scan (RS) FT-IR experiments. The IR spectra were normalised to the standard pellet mass (10 mg). In standard experiments, ethanol ($3{\cdot}10^{-5}$ mol) was introduced to the IR cell at room temperature and contacted with excess oxygen. Then, the temperature was raised successively from room temperature to the desired temperature and the reaction was traced by collecting the respective spectra. Upon reaching the milestone temperatures (50, 100, 150, 200, and 250 °C), the catalysts were cooled to room temperature to

Table 1
Textural properties and chemical composition of the Mn-catalysts and parent zeolites.

Sample	S_{BET} (m^2g^{-1})	Pore volume (m^3g^{-1})	Si/Al molar ratio	Mn (wt %)	Na (wt %)
BEA19	710	0.30	19	-	-
MFI13	425	0.18	12.5	-	-
MFI1000	297	0.14	1000	-	1.0
5MnBEA19	498	0.21	19	5.7	-
5MnMFI13	345	0.15	12.5	5.3	-
5MnMFI1000	291	0.14	1000	5.3	0.8

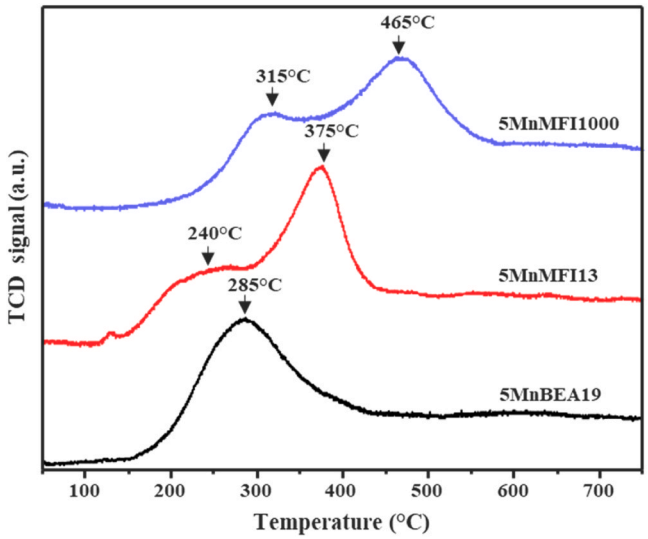

Fig. 1. . TPR profiles of the calcined 5 wt% Mn-catalysts supported on different zeolites.

gather the spectra of adsorbed reagents. In RS FT-IR experiments, the oxidation reaction of ethanol ($3{\cdot}10^{-5}$ mol) was monitored for 300 s at 250 °C.

In *operando* UV–vis studies, the catalyst in the form of a self-supported disc (15–20 mg) was placed in the Praying Mantis™ cell connected to gas-transfer 1/16'' Teflon lines heated at 110 °C to avoid condensation of the reagents. The catalyst was activated at 500ºC using a mixture of 10% oxygen in helium with a total flow of 30 cm^3 min^{-1}. After activation, the temperature was decreased to 200 °C, and the sample was contacted with the reagents (10%O_2 in He, total flow 20 mL/min, 2 mL/min were saturated with ethanol kept at 10 °C) and the UV–vis spectra were taken during ethanol oxidation reaction.

3. Results

3.1. Catalyst characterization

MFI zeolites of significantly different Si/Al ratios (12.5 or 1000) and BEA zeolite were applied to support the active Mn-phase. Textural properties and chemical composition of catalysts and parent zeolites are summarised in Table 1. All samples present Type I isotherms typical of microporous materials. The surface area of the Mn-catalysts is moderately high and varies between 290 and 500 $m^2{\cdot}g^{-1}$. The highest one is found with the catalyst supported on the BEA zeolite and the lowest with the catalyst that has a higher Si/Al ratio. Compared with the parent zeolites, the addition of manganese decreases the surface area and the larger the support surface area, the greater the surface drop after manganese deposition. Nevertheless, XRD patterns show that the zeolite structure was preserved, and no peaks assigned to manganese were found, indicating a good dispersion of the manganese species on the surface (Supporting Information, Figure S1). The micropores volume was fully preserved for 5MnMFI1000, indicating that in this catalyst, manganese is mainly located on the outer surface of zeolite grains.

Table 2
Concentration of Brønsted (B) and Lewis acid sites (L) and acid strength determined from IR spectroscopy measurements with pyridine adsorption/thermodesorption.

Sample	Py [μmol·g^{-1}]			Strength of Lewis acid sites	
	B	L	L+B	$\frac{A_{250}}{A_{150}}$	$\frac{A_{350}}{A_{150}}$
BEA19	395	220	615	1	0.29
5MnBEA19	50	850	900	0.9	0.30
MFI13	650	130	480	1	0.80
5MnMFI13	130	140	270	-	0.12
MFI1000	10	5	20	1	1
5MnMFI1000	0	20	20	1	0.10

TPR of the Mn catalysts are shown in Fig. 1. Two broad peaks appear at different temperatures in the catalysts supported on MFI zeolites. The assignment of these peaks is not straightforward as the reduction of manganese oxides takes place in a sequential mode where MnO_2 is reduced to Mn_2O_3, then to Mn_3O_4 and finally to MnO with overlapping the different peaks [33–35]. According to the literature [36–38], the peak at the lowest temperature corresponds to the reduction of MnO_2/Mn_2O_3 to Mn_3O_4 or the reduction of dispersed MnO_x species [39] and the second peak corresponds to the successive reduction of Mn_3O_4 to MnO. Nevertheless, the manganese oxides formed on the different supports are probably non-stoichiometric systems [40–42] as the broadness and overlapping of the present peaks could indicate. It is observed that the position of the reduction peaks depends on the Si/Al ratio of the zeolites; appearing the peaks at lower temperature when the Si/Al ratio decreases. As the Si/Al ratio is related to the zeolite acidity, these results indicate that a higher number of acid sites favour the reducibility of the supported MnO_x. In the Mn-BEA catalyst only a broad peak around 285 ºC is observed. This peak is characteristic of a highly dispersed manganese oxide phase, probably in 2D epitaxial layers [30]. The hydrogen consumption of the different Mn-zeolites is shown in Supporting Information in Table S1. As it can be seen, the zeolite with the higher Si/Al ratio is the one with maximum hydrogen uptake, suggesting that in this zeolite Mn species with higher oxidation state are formed.

XPS characterization of the Mn-MFI catalysts with different Si/Al was made and the results are shown in Supporting Information (Figure S2). The $Mn2p_{3/2}$ spectra show in both cases the presence of a broad band deconvoluted in three peaks corresponding to Mn^{2+}, Mn^{3+} and Mn^{4+} centred around 640.9 eV, 641.9 eV and 643.1 eV respectively [43]. Although the form of the band is similar in both catalysts, a higher account of Mn^{4+} and Mn^{3+} species are observed in the catalyst with higher Si/Al ratio. Analogous results are described in [43] using similar catalysts, showing that a higher percentage of Mn^{4+} species are associated with higher SiO_2/Al_2O_3 ratio and lower Mn ion content.

The acidic properties of the Mn-catalysts have been studied by pyridine adsorption. Pyridine has a strong Lewis basic character, which makes it useful for discrimination of Lewis and/or Brønsted acid sites on the surface of heterogeneous catalysts [44,45]. In the IR spectrum of adsorbed pyridine, the area between 3000 and 4000 cm^{-1} provides information about the presence of OH groups of different nature present in the solid, while the region between 1400 and 1700 cm^{-1} includes information about the type of acid sites (Lewis or Brønsted) present on the catalyst surface [46]. The appearance of the band around 1450 cm^{-1} is associated with pyridine coordinatively bonded to Lewis acid sites, while the appearance of the band at 1540 cm^{-1} is due to the formation of the pyridinium ion by adsorption of pyridine molecule on Brønsted acid sites.

The difference spectra of pyridine interacting with the acid surface

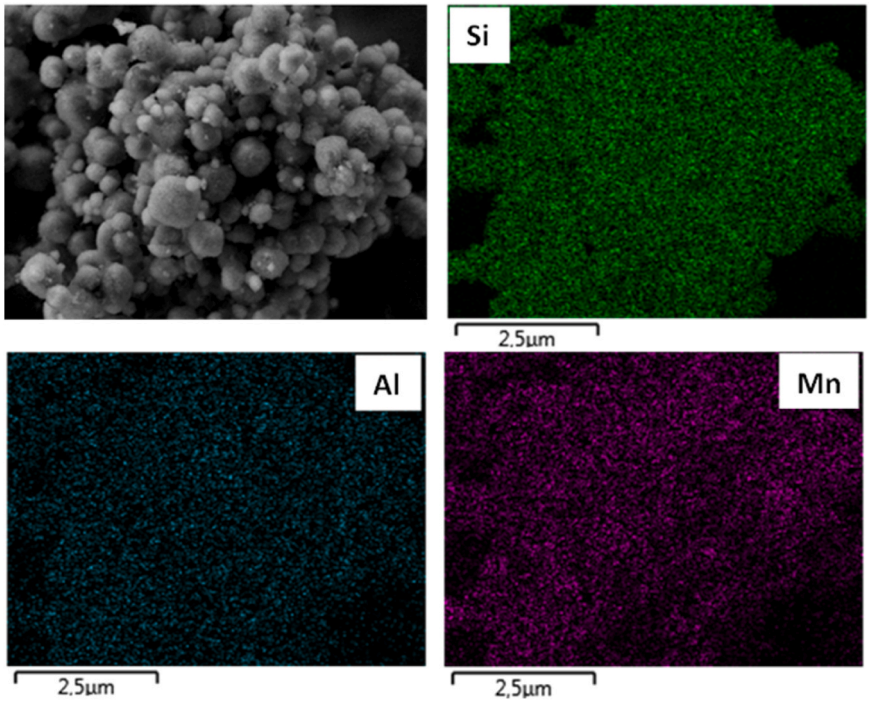

Fig. 2. TEM image and Energy-dispersive X-ray (EDS) mapping analysis of 5MnBEA19.

sites of the Mn-catalysts are shown in Supporting Information, Figure S3, while the concentration of the sites and their strength are given in Table 2. As it can be seen in the table, with all the samples the addition of Mn to the parent zeolite results in an increase of the Lewis acid sites and in a decrease of the Brønsted centers. It also clearly observed that the Mn catalyst supported on the MFI zeolite with lowest Si/Al ratio has more Brønsted and Lewis acid centers than the Mn catalyst supported on the MFI zeolite with higher Si/Al ratio that shows almost no acid sites. The 5MnBEA19 catalyst contains the higher quantity of Lewis acid sites whilst the 5MnMFI13 contains the higher number of Brønsted centres. The relation between the Brønsted acid loss and the number of new sites appearing due to Mn deposition clearly evidences the cationic character

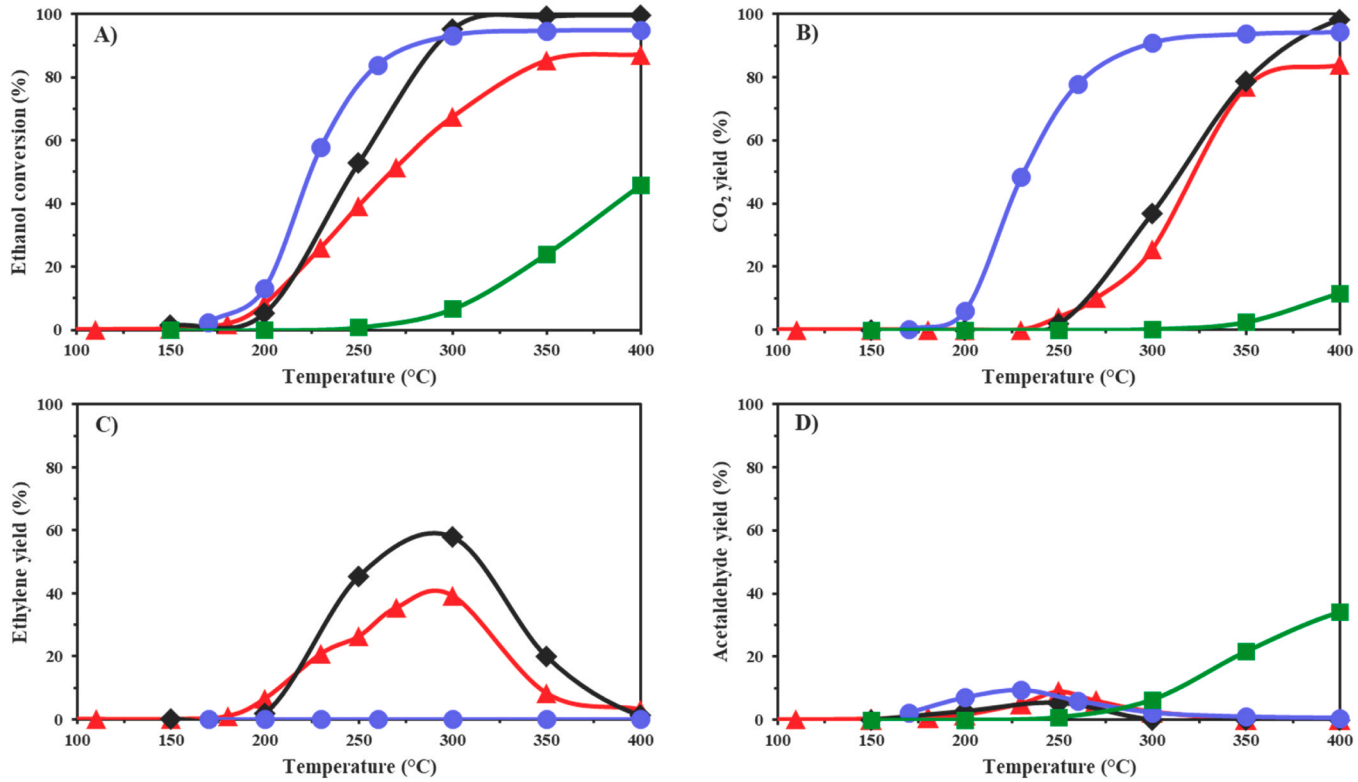

Fig. 3. Catalytic activity for the ethanol oxidation with air at different temperatures and different catalysts: (▲)5MnMFI13, (♦)5MnBEA19, (●)5MnMFI1000, (■) blank. (A) Ethanol conversion; (B) CO_2 yield; (C) Ethylene yield; and (D) Acetaldehyde yield.

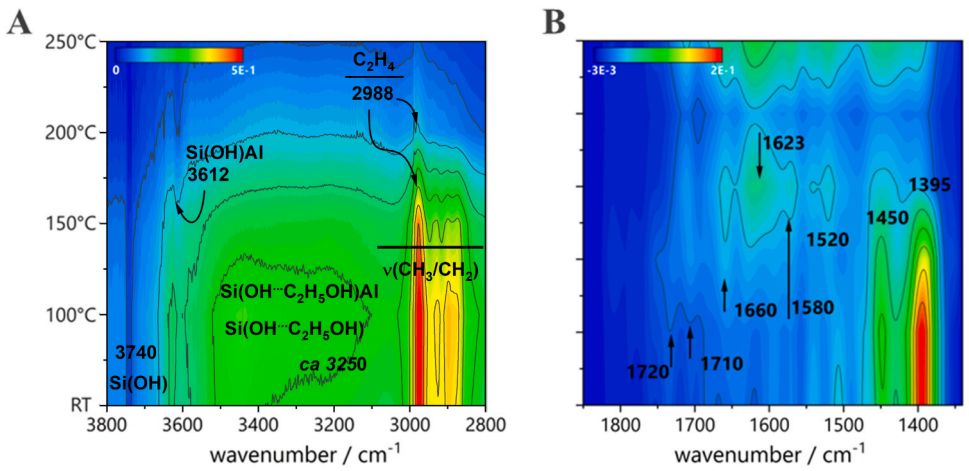

Fig. 4. Top-down projection of the difference spectra in the range of (A) C-H and O-H stretching and (B) C=X (X = C, O) stretching and C-H deformation modes during ethanol oxidation over 5MnMFI13 in the temperature range of RT-250 °C.

of the Mn-species in 5MnBEA19. In 5MnMFI13 a significant loss of protonic sites is also detected but it does not correspond with the number of Mn-originated Lewis sites. Then, it can be inferred that the Mn species in 5MnMFI13 are more significantly clustered than those present in the Mn-BEA catalyst or they have a very weak strength. In 5MnMFI1000, the less dispersed and weakest strength oxo-sites are present. These results confirm that the acidic property of zeolite supports is responsible for the diverse Mn speciation, as provided by TPR studies.

These results are coherent with the characteristics of the different zeolites. In the zeolite with high Si/Al ratio, no metal ion exchange is expected due to the extremely low aluminium content, being the aluminium atoms the sites for the ion exchange. Then in this zeolite more clusters of Mn-oxo species should be formed. On the other hand, in the MFI and BEA zeolite with low Si/Al content, the ionic exchange is possible, probably via a solid ion exchange during the calcination, and in these zeolites, more ionic species are formed as the pyridine experiments have shown. The results also show that the ion exchange is easier in the BEA zeolite than in the MFI zeolite, probably due to the big cavities and larger channels present in the former one.

The HRFESEM-EDS mapping images of the 5MnBEA19 catalyst are presented in Fig. 2. The catalyst has a uniform particle size distribution and a round morphology. Manganese is homogeneously dispersed on the surface of the zeolite without forming important metal agglomerates. Similar results were obtained with the other catalysts.

3.2. Catalytic results

The catalytic activities of the different Mn-zeolites in the oxidation of ethanol at different temperatures and the results obtained in a blank reaction are shown in Fig. 3. As can be seen, the reaction carried out without any catalyst requires significantly higher temperatures for ethanol oxidation, and only the 50% conversion is obtained at 400 ºC. In presence of Mn-catalysts, the oxidation starts at lower temperatures and is almost completed at 350 ºC. The final product obtained is carbon dioxide for all the catalysts, although some primary products, such as ethylene and acetaldehyde, are formed at 150–350 ºC, depending on the catalyst. These molecules are oxidised at higher temperatures to CO_2. Carbon monoxide and acetylene are not formed or are below the detection limit of the gas chromatography. Small amounts of diethyl ether were found for the catalysts with more Brønsted acid sites, i.e. 5MnBEA19 and 5MnMFI13.

As shown in Fig. 3A, the catalyst with the lowest aluminium content, i.e. 5MnMFI1000, is the most active as it requires the lowest temperature for ethanol conversion (T_{50} = 220 ºC). Higher temperatures are necessary for both aluminium-containing catalysts: T_{50} = 250 ºC for the 5MnBEA19 and T_{50} = 270 ºC for the 5MnMFI13 catalyst. It must be pointed out that the most active catalyst is the one with the lowest surface area and the less reducible Mn species. This indicates that other parameters are crucial for designing active catalysts in this reaction. These parameters must be related to the absence of acid sites in the 5MnMFI1000 catalyst. Thus, the different catalyst behaviour must be correlated to the catalyst acidity. This is evidenced when comparing the selectivity of the various catalysts. A complete conversion of ethanol to carbon dioxide (Fig. 3B) is dominant at lower temperatures in the case of 5MnMFI1000, whilst for the samples with Brønsted acidity, CO_2 is only obtained above 250 ºC. On the contrary, ethylene yield is practically absent for 5MnMFI1000, but it is a primary product for 5MnBEA19 and 5MnMFI13 (Fig. 3C), which is later oxidised to CO_2 at temperatures higher than 250 ºC. Acetaldehyde (Fig. 3D) appears as a primary unstable product for all the samples with yields lower than 10%. Nevertheless, the sample 5MnMFI1000 shows the onset at a lower temperature (170 ºC), which indicates that acetaldehyde is a primary unstable product driving to carbon dioxide, whose onset temperature is 200 ºC. This catalyst behaves in selectivity very similarly to other bulk manganese oxide samples referenced in the literature [47], where acetaldehyde is the intermediate product for the complete oxidation of ethanol to CO_2, with low selectivity to carbon monoxide. In the case of the catalysts supported on acid zeolites, in which manganese and Brønsted acidity are present together, a change in the pathway of the reaction is observed. The competitive reaction of ethanol dehydration to ethylene appears [48,49] and delays the total oxidation to CO_2. This is not surprising since removing oxygen from ethanol to give ethylene, followed by oxygen reinsertion to yield CO_2, will require more energy than ethanol's direct oxidation; therefore, a higher temperature will be needed. The combustion of ethylene in Pd/Au catalysts follows a similar route with the formation of ethylene oxide, acetaldehyde and finally CO_2 [50].

The stability of 5MnMFI1000 catalyst was tested by successive reactions with the same catalyst, maintaining its activity after five reaction cycles. This indicates that the catalyst is stable without important deactivation after successive reaction cycles.

The minor differences in the activity of the acid zeolites containing manganese can be related to the zeolites' topology and the Mn-originating species formed on the surface. In the case of 5MnBEA19, a total conversion of CO_2 is reached with a lower T_{50} than for the 5MnMFI13, indicating that the higher accessibility of tridimensional 12-ring zeolite Beta, its higher surface area and the different Mn species formed on this zeolite are more convenient for the ethanol oxidation reaction.

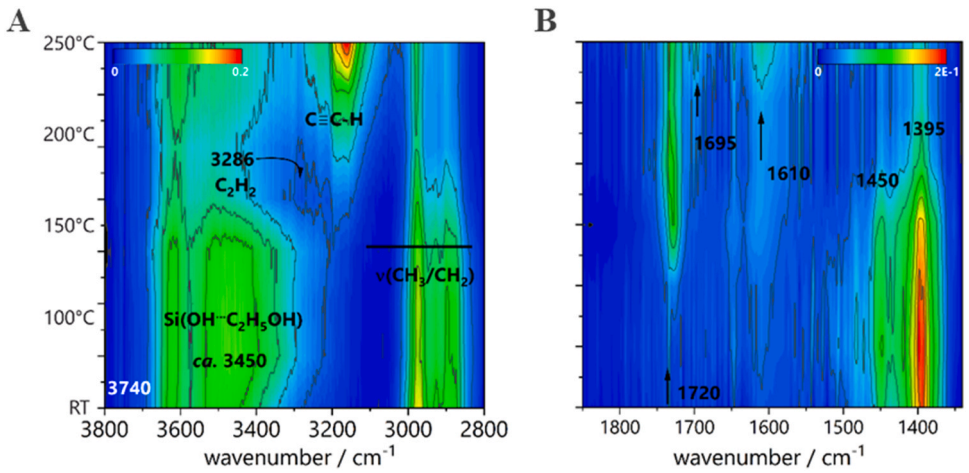

Fig. 5. Top-down projection of the difference spectra in the range of (A) C-H and O-H stretching and (B) C=X (X = C, O) stretching and C-H deformation modes during ethanol oxidation over 5MnMFI1000 in the temperature range of RT-250 °C.

Comparing the results obtained with the 5MnMFI1000 with other supported Mn-catalysts used for the ethanol oxidation, this catalyst shows a high activity (see Supporting Information Table S2) in terms of TOF, although the T_{90} is higher, especially if compared with unsupported MnO_x catalysts.

3.3. IR study of ethanol adsorption and oxidation on Mn-MFI catalysts

The effect of the acidity of the zeolite support on the type of the intermediate species formed and thus on overall activity in the ethanol oxidation was also studied by rapid scan IR spectroscopic studies over Mn-catalysts based on MFI zeolites with different Si/Al ratios.

The results of the infrared study of ethanol adsorption and oxidation at different temperatures with the 5MnMFI13 catalyst are shown in Fig. 4. The spectra presented are the difference spectra in top-down projection. Thus, the adsorbed species are identified as positive bands, while the groups consumed by interaction with the adsorbed reactants are seen as negative. In case that during reaction the consumed groups are restored, these bands become less negative. At room temperature, the interaction of ethanol with the support is recognised by the appearance of CH_3 and CH_2 stretching vibration bands in the frequency range of 3000–2800 cm^{-1} (Fig. 4A) and by the appearance of CH_3/CH_2 deformation vibration bands in the frequency range of 1390–1450 cm^{-1} (Fig. 4B). The most intense band at 1395 cm^{-1} is assigned to ethoxy species. The bands associated with silanol (3740 cm^{-1}) and Si(OH)Al (3612 cm^{-1}) groups of zeolites are consumed due to hydrogen bonding with ethanol. The spectroscopic signature of this interaction is a broad band located ca. 3250 cm^{-1}. No oxidation products are observed at this temperature. At 100 °C, some hydrogen-bonded ethanol molecules are released from silanol groups Si(*OH… C_2H_5OH*), as manifested by restoring the 3740 cm^{-1} band. Nevertheless, the bridging hydroxyls are still engaged in the interaction with ethanol. Most likely, the Si(*OH… C_2H_5OH*)Al species are transformed into ethoxy species, which can be concluded based on many literature data reporting the rapid transformation of alcohols into ethoxy groups even at room temperature [51, 52]. At 150 °C, relatively large amounts of ethylene, identified by the C=C-H at 2988 cm^{-1} and vibrational-rotational spectrum in the 3200–3300 cm^{-1} range, start forming due to dehydration of ethanol over acid sites. At the same time, the disappearance of deformation modes of ethoxy species (1395 cm^{-1}) is accompanied by the evolution of acetaldehyde interacting with Mn cations (1720 cm^{-1}) and acetic acid (1695 cm^{-1}). A complex band centred at ca. 1623 cm^{-1} also appears due to the overlapping of water and acetate bands. The 1660 cm^{-1} band originates from acetate ions produced by the reaction of acetic acid with extra-framework Al species. In the temperature range of 200–250 °C, the bands of acetaldehyde and acetates diminish due to subsequent oxidation to CO_2. Ethylene is still recognised as the only product in C-H stretching modes. Both CO_2 and ethylene (when oxidised) can be accepted as the primary products providing new surface species, i.e. carbonates (1443 and 1400 cm^{-1}) and olefin-aromatic compounds (1650–1500 cm^{-1}), respectively. These results are consistent with those obtained in the catalytic reaction (Fig. 3) of 5MnMFI13, where it was observed that ethylene is a primary product formed at lower temperatures due to ethanol dehydration catalysed by the acid sites. Those results also showed that together with ethylene, acetaldehyde is formed in less extension, and both are oxidised to CO_2 at higher temperatures.

A two-dimensional correlation analysis (2D COS) was coupled with rapid scan time-resolved *in situ* IR spectroscopy for spectra collected at 200 °C to track changes occurring on the catalyst surface. The time evolution of intermediates on the catalyst surface at 200 °C is well visualised in Figure S4 left (supporting material). The surface ethoxy (1375 cm^{-1}) appears on the MnMFI13 surface as the primary species. Acetic acid (1695 cm^{-1}) and acetates of various types (1590, 1580, 1560, and 1518 cm^{-1}) are also produced, but the divergence in the time profiles manifests a noticeable difference in their stability. The amount of acetic acid is meaningful and stable during the reaction. On the other hand, the intensity of the band of acetaldehyde bonded to Mn^{2+} cations (1720 cm^{-1}) is relatively marginal, suggesting rapid oxidation of acetaldehyde to acetic acid. The 2D COS IR data provide more insightful information, as shown in Figure S4 right (supporting material). The acetaldehyde—Mn^{2+}species (1720 cm^{-1}) are negatively correlated with acetic acid (1695 cm^{-1}) and acetates (1590–1560 and 1660 cm^{-1}). These findings indicate that acetic acid and acetate species are produced from acetaldehyde that will be oxidised to CO_2 at higher temperatures, concordant with the previous experiments.

The infrared spectra of ethanol adsorption and oxidation at different temperatures with the 5MnMFI1000 catalyst are shown in Fig. 5. In this material, there is a significant reduction of the acidity that influences the interaction of ethanol molecules with the Mn-catalyst. At room temperature, the ethanol is adsorbed as it is recognised by the CH_3 and CH_2 stretching vibration bands in the frequency range of 2800–3000 cm^{-1} (Fig. 5A) and by the CH_3/CH_2 deformation vibration bands that appear in the range of 1390–1450 cm^{-1} (Fig. 5B). As stated before, the 1395 cm^{-1} band is assigned to ethoxy species. The silanol groups (3740 cm^{-1}) are consumed due to hydrogen bonding with ethanol. The spectroscopic signature of this interaction is a broad band centred at ca. 3450 cm^{-1}. No reaction between ethanol and oxygen is observed at this temperature. The increase in the temperature results in the disappearance of the deformation bands of methyl and methylene groups of ethanol and the development of a band at 1720 cm^{-1} assigned to

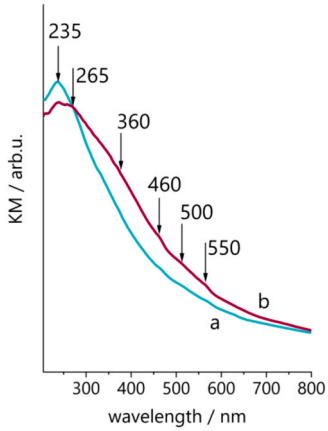

Fig. 6. DR UV–vis spectra collected at 150 °C for 5MnMFI13 (a) and 5MnMFI1000 (b) catalysts O2-pretreated at 500 °C.

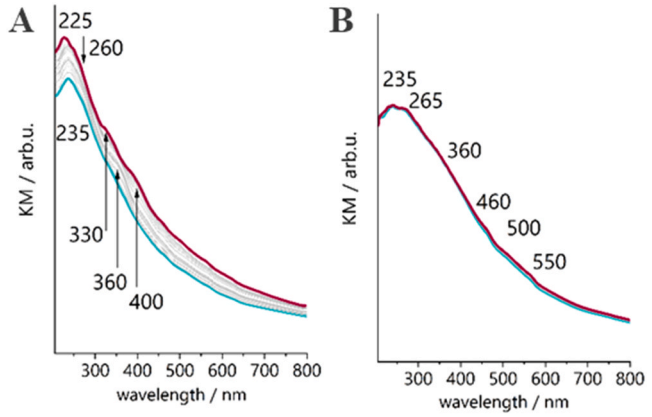

Fig. 7. R UV–vis spectra of the 5MnMFI13 (A) and 5MnMFI1000 (B) contacted with ethanol and oxygen at 200 ºC.

acetaldehyde and a band at 1695 cm^{-1} assigned to acetic acid. It must be pointed out that in contrast to 5MnMFI13, ethylene was not observed among the products over 5MnMFI1000. However, the formation of acetylene is recognised by the 3286 cm^{-1} band. The appearance of coke precursors is not detectable.

The time-dependent profiles of the intermediate species at 200 ºC (Figure S5 left, supporting material) show the formation of ethoxy species (1395 cm^{-1}) as a primary species, which immediately reaches the constant concentration on the zeolite surface. The acetaldehyde, acetylene, and acetates occur later in the reaction. The highest correlation level for acetaldehyde autopeak (1720 × 1720 cm^{-1}) also indicates that this intermediate product is the most abundant and stable (Figure S5 right, supporting material). Although acetylene and acetaldehyde appear on the catalysts simultaneously, the correlations for the acetylene bands were not observed, indicating that acetylene production in the ethanol oxidation process is coincidental without affecting acetaldehyde production. These results are also consistent with those obtained in the catalytic experiments (Fig. 3), observing in both cases the primary formation of acetaldehyde that is oxidised to CO_2 when increasing the reaction temperature.

3.4. UV study of the MnMFI catalysts in ethanol adsorption and oxidation

The DR UV–vis spectra of oxygen pre-treated catalysts are presented in Fig. 6. The broad bands centred at 235 and 265 nm in the UV range are assigned to electron transfer from O^{2-} to tetrahedral isolated Mn^{2+} and Mn^{3+}, respectively [53,54]. The absorption bands at 360 and 460 nm are attributed to the d–d transition of extra-framework Mn^{2+} and Mn^{3+} oxo-species highly dispersed or possibly surface-associated Mn^{3+} [55]. The 500–620 nm bands originate from clustered extra-framework Mn^{3+} and Mn^{4+} [56,57]. The relative contribution of extra-framework Mn^{3+} and Mn^{4+} oxide-like species increases for 5MnMFI1000, as can be deduced from the higher intensities of the bands at 360–620 nm. On the contrary, in 5MnMFI13, the Mn^{2+} (or $Mn^{2+}OH$) cations are stabilised as isolated exchangeable cations as manifested by the high intensity of the 235 nm band. These results are consistent with those obtained by the XPS characterization (figure S2).

An increase in the intensity of the ligand to metal charge transfer $O \rightarrow Mn^{2+/3+}$ band and a shift to lower wavelengths (from 235 to 225–220 nm) is observed upon contact of 5MnMFI13 with ethanol and oxygen mixture at 200 °C (Fig. 7A). This phenomenon can be attributed to the formation of paracetic acid and/or acetates, although the band located at 225 nm may also come from π–π* charge transition in alkenes or conjugated olefins adsorbed on Mn^{2+} sites [58]. An evolution of a new band allocated at 360 nm is detected in the first 5 min of the reaction, and then two new bands at 330 and 400 nm start growing. All these bands arise due to the alteration of ligands located on manganese ions. The 330 nm is due to ethylene binding to the Si(OH)Al sites, while the 360 and 400 nm bands result from ethylene oligomerisation [58].

The species involved in the ethanol oxidation process are represented in the 2D COS UV–vis maps. Positive complex cross-peaks are observed in the synchronous map (Figure S6A left, supporting material). These cross-peaks link the bands of highly dispersed Mn^{2+} and Mn^{3+} oxo-species (330, 360 and 400 nm) and n→π* transitions in acetic acid and/or acetates (260–225 nm). On the other hand, the asynchronous correlations (Figure S6A right, supporting material) confirm that the oligomer accumulation is preceded by ethylene appearance.

The changes in the speciation of manganese species caused by ethanol and oxygen admittance over 5MnMFI1000 are hardly detected in respective DR UV–vis spectra (Fig. 7B). However, it is clear that the changes on the manganese centres undergo a different type than those observed for the MFI zeolite containing aluminium. In this case, the reaction of surface sites with ethanol and oxygen involves mainly the Mn^{4+} oxo-species (460–550 nm) and isolated Mn^{2+} centres (200–210 nm). The negative correlations link the bands representing isolated Mn^{2+} cations and Mn^{4+} oxo-species (Figure S6B supporting material); thus, the reduction $Mn^{4+} \rightarrow Mn^{2+}$ half-cycle is postulated during the reaction. Still, n→π* transitions in acetaldehyde, acetic acid, and acetate species are identified as cross-peaks at 275 nm. Their very low intensities suggest a very weak accumulation of these species on the surface of the Mn-zeolite with a low number of acid centres.

The XPS, UV and TPR characterization of the Mn-MFI catalysts clearly show that different types of manganese sites are formed depending on the acidity of the support. In the less acidic zeolites, Mn-oxo species are formed with higher oxidation states favouring ethanol oxidation. These species seem to be more active than the ionic manganese species, with a lower oxidation state present in the zeolites with lower Si/Al content. These results also indicate that Mn speciation is controlled through the electronic interaction between support and Mn species.

3.5. Reaction mechanism

Comparing the catalytic results with the operando studies on both Mn-catalysts supported on zeolites with different Si/Al ratio, it is observed that the main difference is related to the formation of ethylene and the stability of the acetaldehyde as an intermediate. The presence of the Brønsted acid sites catalyzes the ethanol dehydration at lower temperatures, leading to the formation of ethylene, later oxidized to CO_2 at higher temperatures. In minor quantities, acetaldehyde is also formed and adsorbed on the acid sites, suffering consecutive reactions heading to acetic acid and acetates that, at higher temperatures are oxidized to CO_2 catalysed by the Mn species with ionic character formed on these

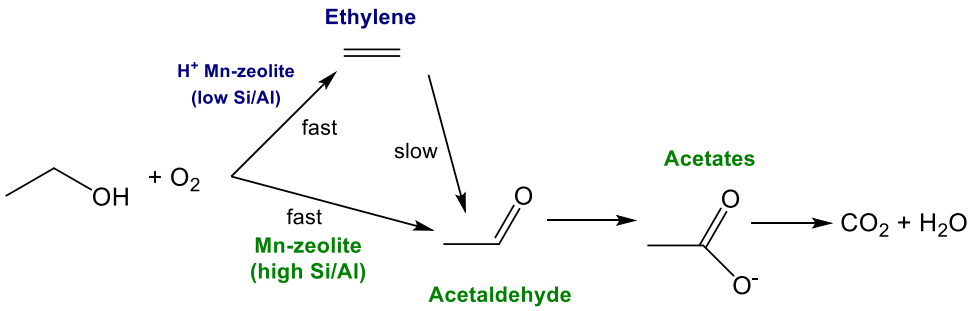

Scheme 1. Different pathway for the oxidation of ethanol on Mn-supported zeolites in the presence (low Si/Al ratio) or absence (high Si/Al ratio) of Brønsted acid sites.

catalysts. On the contrary, the Mn-oxo species with high oxidation state formed on the catalyst with almost no Brønsted acid sites (high Si/Al ratio) enables the transformation of ethanol into acetaldehyde that is directly oxidised to CO_2 without catalysing the dehydration of ethanol into ethylene as it occurs in other Mn-catalysts [20]. The different pathway of the reaction depending on the Si/Al ratio is shown in Scheme 1.

4. Conclusions

The results show that Mn-zeolites are active catalysts for ethanol oxidation, but the activity and selectivity depend on the acidic properties of the zeolite. The extra-framework Al-species play a noticeable role in the retention of acetic acid and CO_2 in the form of carbonates, whereas the Brønsted function is responsible for ethylene production. Then, the dehydration route is inhibited in the catalyst with almost no aluminium and acetaldehyde is initially formed in this catalyst that will be directly oxidised to CO_2 when the temperature increases. The route involving acetaldehyde as an intermediate is faster than the one of the acid catalysts where mainly ethylene is formed below 250 ºC. The ethylene requires higher temperatures to be oxidised to CO_2 than acetaldehyde. The acidity of the support also influences the nature of the Mn-sites, forming more active sites in the catalyst with lower aluminium content. These sites are related to Mn-oxo species with higher oxidation states. Thus, zeolites with higher Si/Al ratios are more adequate for supporting Mn active phase in the reaction of ethanol complete oxidation. This characteristic seems more critical than zeolite topology or catalyst surface area to design active catalysts for complete ethanol oxidation.

CRediT authorship contribution statement

L. Toloza-Blanco: Methodology, Investigation. **K. Góra-Marek**: Writing – original draft, Investigation, Formal analysis. **K. A. Tarach**: Writing – original draft, Formal analysis, Data curation, Conceptualization. **J. Sobalska**: Formal analysis. **J. Martínez-Triguero**: Validation, Supervision, Methodology, Investigation, Data curation, Conceptualization. **A. Plá-Hernández**: Methodology, Data curation. **A. E. Palomares**: Writing – original draft, Supervision, Investigation.

Declaration of Competing Interest

The authors declare that they have no known competing financial interests or personal relationships that could have appeared to influence the work reported in this paper.

Data availability

Catalytic Oxidation of Volatile Organic Compounds with Mn-zeolites - IR and UV-vis original data available in Jagiellonian University Repository; https://doi.org/10.57903/UJ/Q6ZONN.

Acknowledgements

The authors are grateful for the financial support by the Spanish Ministry of Science and Innovation (CEX2021–001230-S grant funded by MCIN/AEI/10.13039/501100011033; TED2021–131715B-I00 grant funded by MCIN/AEI/ 10.13039/501100011033 and by "ERDF A way of making Europe" by the European Union NextGeneration EU/PRTR and PID2021–126235OB-C31). Financial support by the Generalitat Valenciana (Prometeo 2021/077) is also acknowledged. L. Toloza thanks Fundación Carolina for the pre-doctoral grant, call 2019-2020 Universidad Central de Colombia and Universitat Politècnica de València agreement. A. Plá-Hernández thanks Spanish Ministry of Science and Innovation for the pre-doctoral grant PRE2019–088100, associated with the project RTI2018–101784-B-I00. FT-IR and UV–vis in situ and operando studies were financed by Grant No. 2021/41/B/ST4/00048 from the National Science Centre, Poland.

Appendix A. Supporting information

Supplementary data associated with this article can be found in the online version at doi:10.1016/j.cattod.2024.114570.

References

[1] E.V. Makshina, N.S. Nesterenko, S. Siffert, E.A. Zhilinskaya, A. Aboukais, B. V. Romanovsky, Methanol oxidation on LaCo mixed oxide supported onto MCM-41 molecular sieve, Catal. Today 131 (1-4) (2008) 427–430.
[2] P. Lakshmanan, L. Delannoy, V. Richard, C. Méthivier, C. Potvin, C. Louis, Total oxidation of propene over Au/xCeO_2-Al_2O_3 catalysts: influence of the CeO_2 loading and the activation treatment, Appl. Catal. B 96 (1-2) (2010) 117–125.
[3] S. Spatari, Y. Zhang, H.L. MacLean, Life cycle assessment of switchgrass-and corn stover-derived ethanol-fueled automobiles, Environ. Sci. Technol. 39 (2005) 9750–9758.
[4] L. Zou, Y. Luo, M. Hooper, E. Hu, Removal of VOCs by photocatalysis process using adsorption enhanced TiO_2-SiO_2 catalyst, Chem. Eng. Process. 45 (2006) 959–964.
[5] C. Klett, X. Duten, S. Tieng, S. Touchard, P. Jestin, K. Hassouni, A. Vega-González, Acetaldehyde removal using an atmospheric non-thermal plasma combined with a packed bed: role of the adsorption process, J. Hazard. Mater. 279 (2014) 356–364.
[6] J.W. Li, K.L. Pan, S.J. Yu, S.Y. Yan, M.B. Chang, Removal of formaldehyde over $Mn_xCe_{1-x}O_2$ catalysts: thermal catalytic oxidation versus ozone catalytic oxidation, J. Environ. Sci. 26 (12) (2014) 2546–2553.
[7] C.W. Tessum, J.D. Marshall, J.D. Hill, A spatially and temporally explicit life cycle inventory of air pollutants from gasoline and ethanol in the United States, Environ. Sci. Technol. 46 (20) (2012) 11408–11417.
[8] C.P. Cooney, Yeliana, J.J. Worm, J.D. Naber, Combustion characterization in an internal combustion engine with ethanol-gasoline blended fuels varying compression ratios and ignition timing, Energy Fuels 23 (5) (2009) 2319–2324.
[9] A. Aranzabal, B. Pereda-Ayo, M.P. González-Marcos, J.A. González-Marcos, R. López-Fonseca, J.R. González-Velasco, State of the art in catalytic oxidation of chlorinated volatile organic compounds, Chem. Pap. 68 (2014) 1169–1186.
[10] W. Yang, C. Deng, J. Zhou, M. Zhou, Z. Wang, K. Cen, Mesoscale combustion of ethanol and dimethyl ether over Pt/ZSM-5: differences in combustion characteristics and catalyst deactivation, Fuel 165 (2016) 1–9.
[11] R. López-Fonseca, J.I. Gutiérrez-Ortiz, J.R. González-Velasco, Noble metal loaded zeolites for the catalytic oxidation of chlorinated hydrocarbons, React. Kinet. Catal. Lett. 86 (2005) 127–133.
[12] A.J. Schwanke, G.M. Maffi, A. Sachse, C. Radtke, K. Bernardo-Gusmão, R. Balzer, Total oxidation of benzene over cerium oxide-impregnated two-dimensional MWW

zeolites obtained by environmental synthesis using Brazilian rice husk silica agro-industrial waste, Mol. Catal. 529 (2022) 112529.
[13] A.J. Schwanke, R. Balzer, C. Lopes, D. Meira, U. Diaz, A., S. Pergher, A lamellar MWW zeolite with silicon and niobium oxide pillars: a catalyst for the oxidation of volatile organic compounds, Chemistry 26 (2020) 10459–10470.
[14] B. Rivas, R. López-Fonseca, C. Jiménez-González, J.I. Gutiérrez-Ortiz, Synthesis, characterisation and catalytic performance of nanocrystalline Co_3O_4 for gas-phase chlorinated VOC abatement, J. Catal. 281 (1) (2011) 88–97.
[15] A. Gil-Barbarin, J.I. Guttierrez-Ortiz, R. Lopez-Fonseca, B. Rivas, Co_3O_4 hollow nanotubes for the catalytic oxidation of C2-chlorinated VOCs, J. Environ. Chem. Eng. 11 (2023) 109841.
[16] X. Liu, B. Wang, Review on the application of porous minerals in the removal of volatile organic compounds: as adsorbent or catalyst carrier, Pet. Coal 62 (3) (2020) 636–650.
[17] L. Zhang, Y. Peng, J. Zhang, L. Chen, X. Meng, F.S. Xiao, Adsorptive and catalytic properties in the removal of volatile organic compounds over zeolite-based materials, Chin. J. Catal. 37 (6) (2016) 800–809.
[18] J.E. Colman Lerner, M.A. Peluso, A. Porta, H.J. Thomas, J.E. Sambeth, Catalytic removal of a mixture of volatile organic compounds present in indoor air at various work sites over Pt, MnO_x and Pt/MnO_x supported monoliths, Reac Kinet. Mech. Cat. 114 (2015) 395–407.
[19] L. Lamaita, M.A. Peluso, J.E. Sambeth, H. Thomas, G. Mineli, P. Porta, A theoretical and experimental study of manganese oxides used as catalysts for VOCs emission reduction, Catal. Today (2005) 133–138.
[20] M.A. Peluso, E. Pronsato, J.E. Sambeth, H.J. Thomas, G. Busca, Catalytic combustion of ethanol on pure and alumina supported K-Mn oxides: An IR and flow reactor study, Appl. Catal. B 78 (2008) 73–79.
[21] Y. Dai, Y. Men, J. Wang, S. Liu, S. Li, Y. Li, K. Wang, Z. Li, Tailoring the morphology and crystal facet of Mn_3O_4 for highly efficient catalytic combustion of ethanol, Colloids Surf. A Physicochem. Eng. Asp. 627 (2021) 127216.
[22] B. Bai, J. Li, J. Hao, 1D-MnO_2, 2D-MnO_2 and 3D-MnO_2 for low-temperature oxidation of ethanol, Appl. Catal. B 164 (2015) 241–250.
[23] S.S.T. Bastos, J.J.M. Órfão, M.A.A. Freitas, M.F.R. Pereira, J.L. Figueiredo, Manganese oxide catalysts synthesized by exotemplating for the total oxidation of ethanol, Appl. Catal. B 93 (1-2) (2009) 30–37.
[24] S.C. Kim, W.G. Shim, Catalytic combustion of VOCs over a series of manganese oxide catalysts, Appl. Catal. B 98 (3-4) (2010) 180–185.
[25] H. Xu, N. Yan, Z. Qu, W. Liu, J. Mei, W. Huang, S. Zhao, Gaseous heterogeneous catalytic reactions over Mn-based oxides for environmental applications: a critical review, Environ. Sci. Technol. 51 (16) (2017) 8879–8892.
[26] T. Yuranova, C. Franch, A.E. Palomares, E. Garcia-Bordejé, L. Kiwi-Minsker, Structured fibrous carbon-based catalysts for continuous nitrate removal from natural water, Appl. Catal. B. 123-124 (2012) 221–228.
[27] T. Yuranova, L. Kiwi-Minsker, C. Franch, A.E. Palomares, S. Armenise, E. García-Bordejé, Nanostructured catalysts for the continuous reduction of nitrates and bromates in water, Ind. Eng. Chem. Res. 52 (2013) 13930–13937.
[28] M. Moreno-González, A.E. Palomares, M. Chiesa, M. Boronat, E. Giamello, T. Blasco, Evidence of a Cu^{2+}–alkane interaction in Cu-zeolite catalysts crucial for the selective catalytic reduction of NO_x with hydrocarbons, ACS Catal. 7 (2017) 3501–3509.
[29] A. Ayala, G. Fetter, E. Palomares, P. Bosch, CuNi/Al hydrotalcites synthesized in presence of microwave irradiation, Mater. Lett. 65 (11) (2011) 1663–1665.
[30] J. Trawczyński, B. Bielak, W. Miśta, Oxidation of ethanol over supported manganese catalysts—effect of the carrier, Appl. Catal. B 55 (4) (2005) 277–285.
[31] J. Zhang, X. Xu, S. Zhao, X. Meng, F.S. Xiao, Recent advances of zeolites in catalytic oxidations of volatile organic compounds, Catal. Today 410 (2023) 56–67.
[32] K. Sadowska, K. Góra-Marek, J. Datka, Hierarchic zeolites studied by IR spectroscopy: Acid properties of zeolite ZSM-5 desilicated with NaOH and NaOH/tetrabutylamine hydroxide, Vib. Spectrosc. 63 (2012) 418–425.
[33] M. Sun, B. Lan, L. Yu, F. Ye, W. Song, J. He, G. Diao, Y. Zheng, Manganese oxides with different crystalline structures: Facile hydrothermal synthesis and catalytic activities, Mater. Lett. 86 (2012) 18–20.
[34] S. Deng, K. Zhuang, B. Xu, Y. Ding, L. Yu, Y. Fan, Promotional effect of iron oxide on the catalytic properties of Fe–MnO_x/TiO_2 (anatase) catalysts for the SCR reaction at low temperatures, Catal. Sci. Technol. 6 (2016) 1772–1778.
[35] N. Fang, J. Guo, S. Shu, H. Luo, Y. Chu, J. Li, Enhancement of low-temperature activity and sulfur resistance of $Fe_{0.3}Mn_{0.5}Zr_{0.2}$ catalyst for NO removal by NH_3-SCR, Chem. Eng. J. 325 (2017) 114–123.
[36] E.R. Stobbe, B.A. de Boer, J.W. Geus, The reduction and oxidation behaviour of manganese oxides, Catal. Today 47 (1999) 161–167.
[37] R. Fiorenza, L. Spitaleri, A. Gulino, S. Scirè, Ru-Pd bimetallic catalysts supported on CeO_2-MnO_x oxides as efficient systems for H_2 purification through CO preferential oxidation, Catalysts 8 (5) (2018) 203.
[38] Y.B. Tu, J.Y. Luo, M. Meng, G. Wang, J.J. He, Ultrasonic-assisted synthesis of highly active catalyst Au/MnO_x–CeO_2 used for the preferential oxidation of CO in H_2-rich stream, Int. J. Hydrog. Energy 34 (2009) 3743–3754.
[39] F.N. Aguero, A. Scian, B.P. Barbero, L.E. Cadús, Influence of the support treatment on the behavior of MnO_x/Al_2O_3 catalysts used in VOC combustion, Catal. Lett. 128 (2009) 268–280.
[40] S.S.R. Putluru, L. Schill, A.D. Jensen, B. Siret, F. Tabaries, R. Fehrmann, Mn/TiO_2 and Mn–Fe/TiO_2 catalysts synthesized by deposition precipitation-promising for selective catalytic reduction of NO with NH3 at low temperatures, Appl. Catal. B 165 (2015) 628–635.
[41] X. Wang, S. Wu, W. Zou, S. Yu, K. Gui, L. Dong, Fe-Mn/Al_2O_3 catalysts for low temperature selective catalytic reduction of NO with NH_3, Chin. J. Catal. 37 (8) (2016) 1314–1323.
[42] B. Thirupathi, P.G. Smirniotis, Co-doping a metal (Cr, Fe, Co, Ni, Cu, Zn, Ce, and Zr) on Mn/TiO_2 catalyst and its effect on the selective reduction of NO with NH_3 at low-temperatures, Appl. Catal. B 110 (2011) 195–206.
[43] H. Wang, B. Peng, R. Zhang, H. Chen, Y. Wei, Synergies of Mn oxidative ability and ZSM-5 acidity for 1, 2-dichloroethane catalytic elimination, Appl. Catal. B 276 (2020) 118922.
[44] J. Lercher, C. Grundling, G. Eder-Mirth, Infrared studies of the surface acidity of oxides and zeolites using adsorbed probe molecules, Catal. Today 27 (3-4) (1996) 353–376.
[45] M.R. Basila, T.R. Kantner, K.H. Rhee, The nature of the acidic sites on a silica-alumina. characterization by infrared spectroscopic studies of trimethylamine and pyridine chemisorption1, J. Phys. Chem. 68 (11) (1964) 3197–3207.
[46] E.P. Parry, An infrared study of pyridine adsorbed on acidic solids. Characterization of surface acidity, J. Catal. 2 (5) (1963) 371–376.
[47] S. Chen, H. Li, Y. Hao, R. Chen, T. Chen, Porous Mn-based oxides for complete ethanol and toluene catalytic oxidation: The relationship between structure and performance, Catal. Sci. Technol. 10 (2020) 1941–1951.
[48] F.F. Madeira, N.S. Gnep, P. Magnoux, S. Maury, N. Cadran, Ethanol transformation over HFAU, HBEA and HMFI zeolites presenting similar Brønsted acidity, Appl. Catal. A: Gen. 367 (2009) 39–46.
[49] K. Gołąbek, K.A. Tarach, U. Filek, K. Góra-Marek, Ethylene formation by dehydration of ethanol over medium pore zeolites, Spectrochim. Acta Part A Mol. Biomol. Spectrosc. 192 (2018).
[50] Y. Gao, X. Huo, T. Li, R. Jiang, Q. Zhu, H. Ren, Mechanisms and energetics of complete ethylene oxidation on a PdAu bimetallic catalyst from a theoretical perspective, J. Phys. Chem. C. 126 (22) (2022) 9361–9370.
[51] W. Wang, J. Jiao, Y. Jiang, S.S. Ray, M. Hunger, Formation and decomposition of surface ethoxy species on acidic zeolite Y, ChemPhysChem 6 (2005) 1467–1469.
[52] J.N. Kondo, K. Ito, E. Yoda, F. Wakabayashi, K. Domen, An ethoxy intermediate in ethanol dehydration on Brønsted acid sites in zeolite, J. Phys. Chem. B 109 (2005) 10969–10972.
[53] S. Velu, N. Shah, T.M. Jyothi, S. Sivasanker, Effect of manganese substitution on the physicochemical properties and catalytic toluene oxidation activities of Mg-Al layered double hydroxides, Microporous Mesoporous Mater. 33 (1-3) (1999) 61–75.
[54] N.N. Tušar, S. Jank, R. Gläser, Manganese-containing porous silicates: synthesis, structural properties and catalytic applications, ChemCatChem 3 (2) (2011) 254–269.
[55] H. Xin, J. Zhao, S. Xu, J. Li, W. Zhang, X. Guo, E.J.M. Hensen, Q. Yang, C. Li, Enhanced catalytic oxidation by hierarchically structured TS-1 zeolite, J. Phys. Chem. C. 114 (14) (2010) 6553–6559.
[56] W.S. Kijlstra, E.K. Poels, A. Bliek, B.M. Weckhuysen, R.A. Schoonheydt, Characterization of Al_2O_3-supported manganese oxides by electron spin resonance and diffuse reflectance spectroscopy, J. Phys. Chem. B 101 (3) (1997) 309–316.
[57] T. Takashima, K. Hashimoto, R. Nakamura, Inhibition of charge disproportionation of MnO_2 electrocatalysts for efficient water oxidation under neutral conditions, J. Am. Chem. Soc. 134 (44) (2012) 18153–18156.
[58] J. Melsheimer, D. Ziegler, Ethene transformation on HZSM-5 studied by combined UV–VIS spectroscopy and on-line gas chromatography, J. Chem. Soc. Faraday Trans. 88 (14) (1992) 2101–2108.